DOI: 10.21776/ub.jpacr.2016.005.03.291 *J. Pure App. Chem. Res.*, **2016**, 5 (3), 162-172
5 October 2016

Depth Profiling of Dark and Light Green Bacan: Construction of Material Characters Models from Elemental Analysis and Mineralogical Characterization

Rizky Arief Shobirin[1,2,*] and Abdul Malik Bahrudin[1]

[1]Departement of Chemistry, Faculty of Mathematics and Natural Sciences, University of Brawijaya
[2]Study Centre of Civilisation, University of Brawijaya

[*]Corresponding author : rashobirin@gmail.com Tel. : +6281230667139; Mobile : +6285815434429

Received 8 July 2016; Revised 22 September 2016; Accepted 5 October 2016

ABSTRACT

We have demonstrated the evolutional depth profiling methods for local minerals of Bacan in order to establish the sold price and maintenance of minerals sector in Indonesia. The depth profiling methods was performed by elemental analysis and mineralogical characterisation using X-ray fluorescence (XRF) and X-ray diffraction (XRD). We refined materials parameters then constructed the materials models to describe the difference of materials characters. These results described that LG Bacan has crystals phase of Dioptase ($CuSiO_3$), Liebenbergite (Ni_2SiO_4), and variant of Calderonite ($Ca_2CuP_2O_9$). DG Bacan has crystals phase of Fayalite (Fe_2SiO_4), and variant of Ferriannite ($KCaFe_3Si_3O_{12}$). All crystals phase in LG Bacan has growth orientation on [001] direction, and has more structured crystallite size with small range of its distribution. All phase in DG Bacan has the preferred growth so, except Fayalite crystal phase. DG Bacan less structured than LG Bacan, with wider range of crystallite size distribution, but has harder structure than LG Bacan. Quartz structure in LG Bacan was more polar than DG Bacan.

Keywords: Bacan, Mineralogical Characterisation, Elemental Analysis, XRF, XRD, Materials Modeling

INTRODUCTION

Mineral, as one of the mining materials, is one of the most important aspects in the economy and social development of a country. The mining products are widely used as a starting material in the manufacturing of applied material such as parts of electronic devices or even simply for jewels. However, the abundance of such minerals is limited [1]. Therefore, the government needs impose some regulations to control their exploitation, which might cause a drastic decreasing of mineral resources.

One of the highest abundance of minerals in the Earth is silicates, which is about ~25%, which have high levels of hardness about 6-7 mohs's scale. Quartz is the second most abundance silicate mineral in Earth. This mineral has properties such as piezoelectricity, optical activity, and enantiomorphism [2]. These properties cause quartz become the most sought materials after not only because of the beautiful appearance but also it can alter a polar tension into an electric charge, and vice versa. The mineral is potential to be applied to the field of optics and electronics applications, such as ultrasonic generators, amplifiers, microphones, and quartz-time pieces [3].

The journal homepage www.jpacr.ub.ac.id
p-ISSN : 2302 – 4690 | e-ISSN : 2541 – 0733

In Indonesia, one of the quartz mineral which is most sought after is Bacan. Bacan is a quartz mineral that is vastly found in Bacan Island and Maluku. Generally, Bacan have green colour with various brightness levels [4]. Its high aesthetic value causes this mineral as the most sought after and sold in various range of prices especially in Indonesia. A standard selling price is needed in order to maintain its market values as well as improve the welfare of Indonesian people. Common methods of mineral analysis which used to certificate the minerals as jewels is only using simple physical methods by mineralogists, such as shape, size, colour, and cleavage. These methods are helping to raising the selling price of minerals, but insignificant. In-depth analysis of the Bacan properties is conducted. The sophisticated depth profiling of Bacan by mineralogy and elemental analysis can be used to establish the mineral process and sold price to be significant in international market.

MATERIALS AND METHODS

Minerals Sampling

Bacan minerals were randomly collected from Kasiruta Island mining area, South West Halmahera, Maluku, Indonesia. For the sampling selection, only two kinds of Bacan minerals (as Dark Green (DG) and Light Green (LG) Bacan) were chosen because of their appearance in most in jewel market places in Indonesia. The Bacan samples were cleaned by purified water then polished using smooth-cleaner brush to remove surface impurities.

Elemental Analysis and Mineralogical Characterisation

Each of the DG and LG Bacan were separately grinded to be smaller size for sample preparation. The samples were sent to Central Laboratory at University of Malang (East Java) for elemental analysis. XRF (x-ray fluorescence) PANalytical type Minipal 4 were used to analyse the element abundance in the samples. Furthermore, some of the samples were characterised using XRD (x-ray diffraction) powder method for mineral analysis. The XRD instrument used was PHILIPS-Xpert MPD with X-ray wavelength of 1.540598 Å, and the collection was done in the diffraction angle from 5 to 55˚. These profiling methods were verified by IR spectra which performed using fourier transform-infra red instrument of FTIR-8601PC.

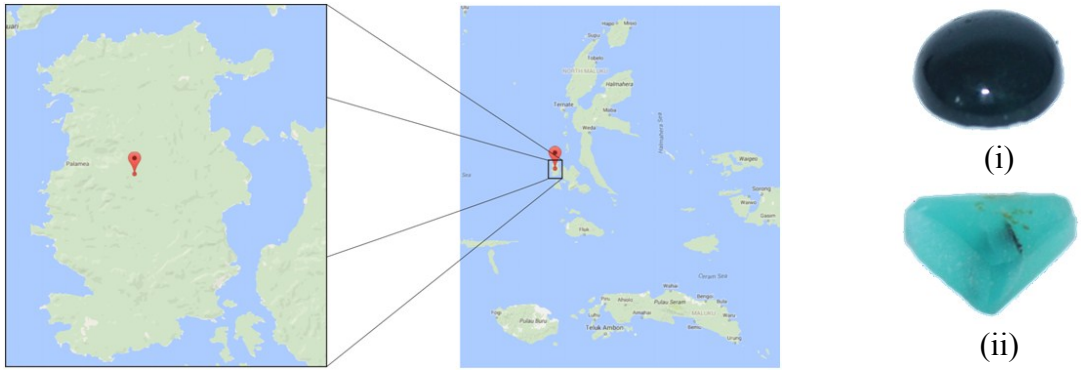

Figure 1. **(a)** The mining location maps located in Kasiruta Island (*left – inset*), South West Halmahera, Province of Maluku (*right*), Indonesia. (b) (i) Dark Green Bacan; (ii) Light Green Bacan.

Material Modeling

Construction of the mineral models performed using Rietveld refinement method from each diffractogram of the Bacan minerals. The refinement process was performed using freely available software Rietica (ver. 1.7.7) under Voigt peak shape profile (Howard asymmetry), and March-Dollase model [5-8]. The ICSD standards which have been used as reference structure models are ICSD #16596 (Tetraferriannite), ICSD #98790 (Calderonite), ICSD #68762 (Fayalite), ICSD #174 (Low-Quartz), ICSD #89669 (Dioptase), and ICSD #4337 (Liebenbergite) [9-14]. From the refinement process, it could be obtained accurate values of lattice parameter, atomic coordinates and their displacement values, and preferred orientation. Then, the crystal structure models were constructed which described the material characters from its inter-atomic distance, until the representative crystal structure model with its crystallite size distribution. The construction of crystal structure models were performed using freely software XtalDraw with lattice parameter and atomic coordinates as data input. Crystal shape models were constructed by freely software WinXMorph with input preferred orientation data [15-17].

FWHM (full width at half-maximum peak/β) at specific miller indices were measured using lorentzian peak function (eq. 1), where X and Y were refined parameters. Crystallite size (L) was measured from eq. (2), where used β values were followed the released value from eq. (1).

$$\beta = \frac{X}{\cos\theta} + Y \tan\theta \quad (2)$$

$$L = \frac{K\lambda}{\beta \cos\theta} \quad (3)$$

K is Scherrer constant (K value is 0.9 for hexagonal and trigonal crystal form), θ is a half of diffraction angles, and λ is x-ray wavelength [18]. From calculated values of average crystallite size and strain from eq. (1) and (2), crystallite size distribution were modelled using Gaussian distribution statistical method, which shown in eq. (4) [19]. Distributions of crystallite size as spherical shape were calculated using Gaussian distribution statistical method, as shown in eq. (3) and (4), ($\bar{L}$)

$$f(L) = \frac{1}{L}\frac{1}{2\pi a}\, e^{-\left(\frac{L\sqrt{a}}{\bar{L}a^2}\right)^2} \quad (4)$$

Where $a = (1+(\sigma_L^2/\bar{L}^2))$. L and $\bar{L}$ are observed and average crystallite size (nm), respectively, and its standard deviation (σ). By combining all of crystallite sizes of all crystals phase with its standard deviation, it could be distributed overall crystallite size which statistically described as mixture crystallite size distributions function of all crystals phase.

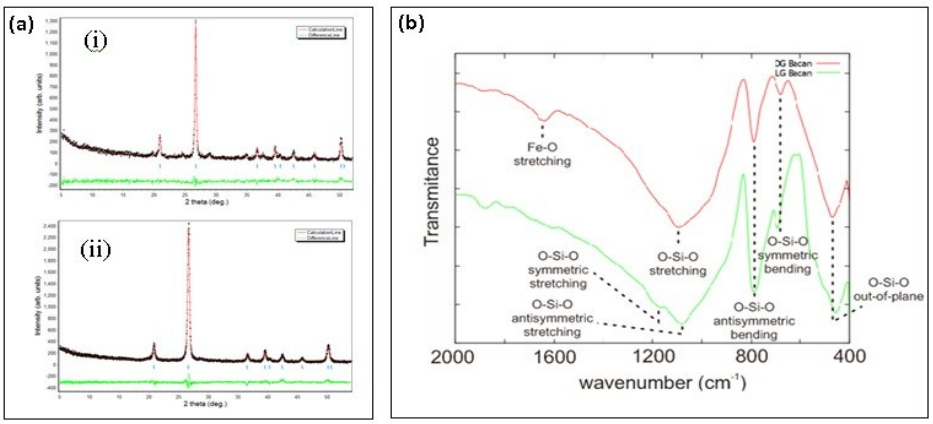

Figure 2. (Right) **(a)** Refinement results of XRD patterns (*bottom*) of polished **(i)** DG, and **(ii)** LG Bacan minerals. **(b)** IR spectra comparison of DG and LG Bacan.

RESULT AND DISCUSSION

Mineralogy and Elemental Analysis

From the shapes of both Bacan types (**figure 1b**), there were differences in colour and clarity, and have differences in material hardness level, which were 6 mohs for LG Bacan, and 6.5 mohs for DG Bacan. The colour of DG Bacan was dark green, while the LG Bacan colour was turquoise, with blue as a base colour that approached to green colour. The brightness difference is due to the content of the different elements on each mineral. DG and LG Bacan's colour were green due to the Ni element content. The content of Ni in LG Bacan was higher than DG Bacan, so that the green colour was more visible. DG Bacan's colour was darker than the LG Bacan because the Fe content was much higher by a margin of ~27%, as presented in **table 3**. However, what makes the characteristic turquoise colour in LG Bacan was the high content of Cu. Turquoise to be green colour was owned by LG Bacan due to the high Cu content then combined with the presence of Ni [20]. Brightness on the LG Bacan was higher, due to the higher Si content which formed SiO_2 compounds and low impurities (**table 3**). SiO_2 was the highest content of both types of Bacan, so SiO_2 was a form of the primary structure of these two types of Bacan. The content of other elements (**table 3**) will affect the shape of the crystal structure of each mineral Bacan.

Table 1. Refined result parameters of DG Bacan (R_p 10.581%; R_{wp} 13.211%; χ^2 1.320)

Phase	SiO_2				$KCaFe_3Si_3O_{12}$				Fe_2SiO_4			
SG*	*P* 3_2 2 1				*C* 1 2/*m* 1				*P b n m*			
PS*	0.0004615				0.00043316				0.000155434			
Lattice Par.	***a***	4.9116	*α*	90	***a***	5.2317	*α*	90	***a***	4.9878	*α*	90
	b	4.9116	*β*	90	***b***	9.0264	*β*	100.71	***b***	10.55	*β*	90
	c	5.4054	*γ*	120	***c***	10.183	*γ*	90	***c***	6.1434	*γ*	90
Atom pos.		***x***	***y***	***z***		***x***	***y***	***z***		***x***	***y***	***z***
	Si	0.5003	0	0.6667	**K**	0	0.5	0	**Fe**	0	0	0
	O	0.4115	0.2557	0.7658	**Ca**	0	0	0.5	**Fe**	-0.0955	0.2421	0.25
					Fe	0	0.3135	0.5	**Si**	0.4367	0.0735	0.25
					Fe	0.5730	0.3121	0.2453	**O**	0.7538	0.0335	0.25
					Si	0.5631	0.3008	0.2206	**O**	0.2934	-0.0411	0.25
					O	0.6204	0	0.3956	**O**	0.3455	0.1565	0.0536
					O	-0.0549	0	0.1706				
					O	0.8547	0.2577	0.1667				
					O	0.6377	0.3115	0.4005				
PO* [hkl]	[001]		***r***	0.94468	**PO [hkl]**	[001]	***r***	0.94468	**PO [hkl]**	[001]	***r***	0.94468

*SG : space group, *PS : Phase scale, *PO : Preferred orientation

Table 2. Refined result parameters of LG Bacan (R_p 10.010%; R_{wp} 13.160%; χ^2 1.934)

Phase	SiO_2				Ni_2SiO_4			
SG*	*P* 3_2 2 1				*F d* -3 *m*			
PS*	0.0011092				0.000034298			
Lattice Par.	***a***	4.9211	*α*	90	***a***	7.6735	*α*	90
	b	4.9211	*β*	90	***b***	7.6735	*β*	90
	c	5.3985	*γ*	120	***c***	7.6735	*γ*	90
Atom pos.		***x***	***y***	***z***		***x***	***y***	***z***
	Si	0.4859	0	0.6667	**Ni**	0.125	0.125	0.125
	O	0.4194	0.2705	0.7890	**Si**	0	0	0
					O	0.3753	0.3753	0.3753
PO* [hkl]	[001]		***r***	0.81126	**PO [hkl]**	[001]	***r***	0.81349
Phase	$CuSiO_3$				$Ca_2CuP_2O_9$			
SG*	*P b m m*				*P* 1 2_1/*m* 1			
PS*	0.000122414				0.00020737			
Lattice Par.	***a***	4.5064	*α*	90	***a***	8.0175	*α*	90
	b	8.5752	*β*	90	***b***	6.2833	*β*	114.15
	c	2.9132	*γ*	90	***c***	8.881	*γ*	90

Atom pos.		*x*	*y*	*z*		*x*	*y*	*z*		*x*	*y*	*z*
	Cu	0.5	0	0	**Ca**	0.3382	0.75	0.3775	**O**	0.4281	0.75	0.9348
	Si	0.0870	0.25	0.5	**Cu**	0	0	0	**O**	0.7968	0.75	0.9345
	O	0.9732	0.25	0	**P**	0.9575	0.75	0.6658	**O**	0.7294	0.75	0.5070
	O	0.2796	0.0926	0.5	**Ca**	0.6911	0.75	0.1705	**O**	-0.0090	0.0309	0.2312
					P	0.5577	0.75	0.8032	**O**	0.0715	0.75	0.5447
					O	0.5005	0.9603	0.7187	**O**	0.1743	0.75	0.0868
PO* [hkl]	[001]		***r***	0.73818	**PO [hkl]**	[001]	***r***	0.97146				

Table 3. Element abundance of DG and LG Bacan obtained from XRF and theoretically calculated from XRD

DG Bacan				LG Bacan		
Basic Elements	**by XRF (%)**	**by XRD (%)**		**Basic Elements**	**by XRF (%)**	**by XRD (%)**
Si	57.30	66.72		Si	72.80	82.81
Fe	28.00	25.74		Cu	7.70	7.50
K	6.13	3.77		Ni	1.86	2.09
Ca	6.68	3.77		Ca	6.81	3.80
				P	8.50	3.80
Other Elements	**by XRF (%)**	**Other Elements**	**by XRF (%)**	**Other Elements**	**by XRF (%)**	
Ba	0.20	Cr	0.09	Ba	1.00	
Cu	0.20	Mn	0.12	Fe	0.61	
Ni	0.26	Sr	0.47	Cr	0.32	
V	0.05	Yb	0.10	Os	0.30	
Ti	0.55			Ti	0.07	

Material Characters and Models

Crystal Structure Models

DG and LG Bacan minerals had the same most abundance crystal phase; they are Quartz (SiO_2). Based on the space group, the two Bacan minerals had the material characters, which are non–centrosymmetric, enantiomorphism, piezoelectric, and optical activity. The both have been observed throughout the data refinement of XRD patterns (**fig. 2a**) which were identical to the ICSD #174, with its results were described in **table 1** and **2**, and simulated in **figure 4** [12].

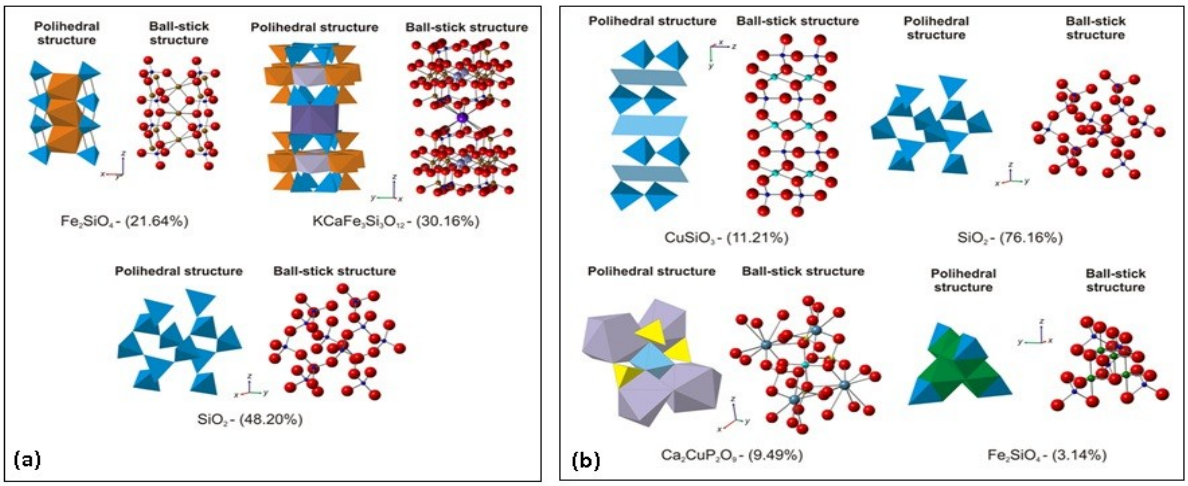

Figure 4. Crystal structures with polyhedron and ball-stick representation and their compounds abundances of **(a)** DG Bacan, and **(b)** LG Bacan. All the structures were constructed from data which listed in **table 1** and **2**.

All these results were confirmed with IR spectra (**fig. 1b**) which showed O–Si–O stretching and bending in region of 1200-1100 and 800-600 cm^{-1}, respectively. IR spectra in **figure 2b** showed that the DG Bacan have more similar Si–O bonds than LG Bacan, which showed only a peak of O–Si–O stretching at 1093.57 cm^{-1} and lower O–Si–O bending at 788.83 and 678.90 cm^{-1}. LG Bacan has different Si–O which is showed by O–Si–O base peak and its shoulder at 1168.78 and 1081.99 cm^{-1}, respectively.

Each of Bacan minerals has other crystals phase which has contribution to their physical appearance, hardness level, and characters. LG Bacan has Dioptase ($CuSiO_3$) which have contribution to releasing turquoise colour, small abundance of Liebenbergite (Ni_2SiO_4) which have releasing green colour, and variant of Calderonite ($Ca_2CuP_2O_9$) [13,14]. DG Bacan has Fayalite (Fe_2SiO_4) which has releasing green-to-dark brown colour and strong hardness level (6.5 mohs), and variant of Ferriannite ($KCaFe_3Si_3O_{12}$) has contribution to release brownish-black colour [9, 11].

Crystallographic Characters from Geometrical Studies

Each point groups has essential material characters based on their geometrical studies. It should be analysed for knowing which minerals have prospective characters to be applied in electrical field, for example as low-cost thin film substrate [21]. Obtained crystals phase in DG and LG Bacan has specific point groups, which represents their material characters specifically, as shown in **table 4**. From the material characters, it can be concluded that only Quartz (SiO_2) phase which has piezoelectric, optical activity, and enantiomorphism characters. From this Quartz phase, further it can be measured geometrically for its polarity through inter-atomic bond lengths observation. Representation of these parameters provided information related to the inter-atomic bond lengths (covalent bonding and dipole moment). The bond lengths were obtained from simulated molecular structure observation which presented in **figure 5**.

Table 4. Crystallographic characters of each crystals phase

Material Characters	SiO_2	$KCaFe_3Si_3O_{12}$	Fe_2SiO_4	$Ca_2CuP_2O_9$	Ni_2SiO_4	$CuSiO_3$
Point Group	32	2/*m*	*m m m*	2/*m*	*m* -3 *m*	*m m m*
Piezoelectric	+	-	-	-	-	-
Optical Activity	+	-	-	-	-	-
Enantiomorphism	+	-	-	-	-	-
Pyroelectric	-	-	-	-	-	-

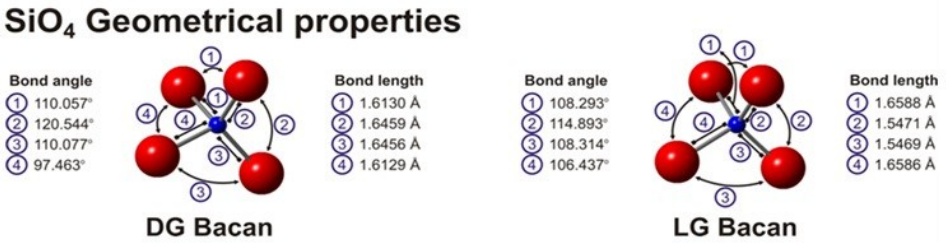

Figure 5. SiO_4 coordination bonding of SiO_2 crystal phase which represented from DG and LG Bacan.

LG Bacan had covalent bond lengths of Si–O shorter (position (**2**) and (**3**) in **figure 5** right), but the dipole moment bonds of Si–O (position (**1**) and (**4**) in **figure 5**-right) inter-molecules of SiO_2 were longer than DG Bacan (**figure 5**-left). Overall, LG Bacan had

difference of inter-atomic bond lengths of Si–O (as polar covalent bonding and coordination bonding) were higher than DG Bacan (**figure 5**-left). The large difference indicates that the degree of symmetry of the SiO_2 structure of LG Bacan lower than DG Bacan. According to the VSEPR theory, higher the degree of symmetry of molecular structure, lower the polarity level of the molecular structure [22]. From the comparison of the bond lengths and angles, could be simulated the degree of symmetry by using a distortion parameter (DP) of molecular structure, which is generally defined in eq. (5).

$$DP = \frac{(Si{-}O)_{long} - (Si{-}O)_{short}}{(Si{-}O)_{long} + (Si{-}O)_{short}} \quad (5)$$

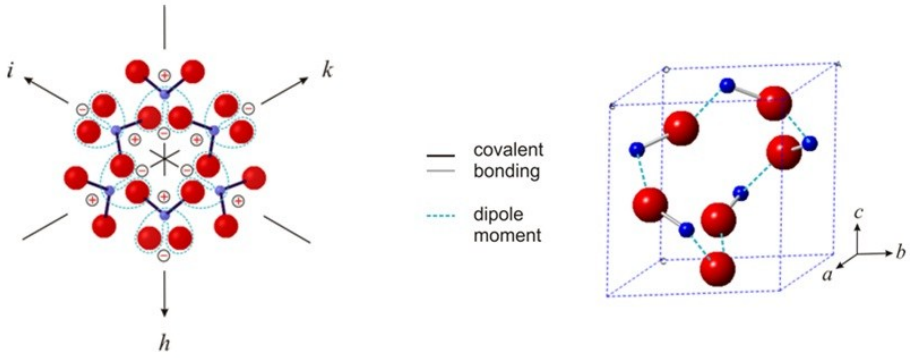

Figure 6. Simulation of **(a)** polar tensors (viewed from [0001]), and **(b)** axial tensors of SiO_2 in a unit cell, which reflects the characters of piezoelectric and optical activity, respectively.

The DP of LG Bacan was higher (0.03491) than DG Bacan (0.01013). Higher distortion level of LG Bacan described LG Bacan was more asymmetric which caused more polar. Higher polarity level and lower degree of symmetry of LG Bacan provided information that its piezoelectricity and optical activity were higher than DG Bacan. Piezoelectric characters exist in a material due to the asymmetry of charge distribution along an axis (**figure 6a**). Higher distortion level of atomic positions of Si atom towards O atom which have polar covalent bonds and the dipole moment caused lower the degree of symmetry. The low degree of symmetry caused high asymmetric distribution of charges along an axis, so that the molecular structure was polar structure. The presence of polar tensor could cause the crystal to vibrated, so that when the crystals were given an electric field will automatically structuring charge happen following the direction of applied electric field. The electric field of a certain direction would cause the compression or tension. It was also the opposite occurs, i.e. when the compression or tension applied to the crystal from a certain direction, would produce positive and negative electric charge in a parallel and anti-parallel position follow the direction. On DG Bacan, its piezoelectricity level was lower and angles difference of covalent bond and dipole moment of Si with O were lower, so the degree of symmetry was higher. High degree of symmetry was almost identical to β-quartz (high-quartz), which was close to be centro-symmetric structure [23]. This made its piezoelectricity level decreased, because the charge distribution along an axis to be symmetrical crystal structure that caused it to become less polar structure.

Structural tetrahedron spiral of SiO_2 (point group 32 - symmetry operation D_3) of LG and DG Bacan minerals reflect chiral and enantiomorphism characters, so these argue that optical activity characters were present in these Bacan minerals. The optical activity character is related to the symmetry of the unit cell, so that the difference of the atom position impacts

to inter-atomic bonding patterns which formed in a unit cell. The pattern of chiral inter-atomic bonds with different bond angles caused their inter-atomic axial tensor towards a certain direction and did not reverse direction (**figure 6b**) [23]. The difference of inter-atomic bonds of LG Bacan which higher than DG Bacan provides information that SiO_2 structure on the LG Bacan was more chiral than DG Bacan. This caused inter-atomic axial tension become higher and could rotate the plane of polarised light which beamed to the SiO_2 crystal structure. The colour of transmitted polarised light along *c*-axis direction is depending on the the wavelength of the light. It has been confirming generally why the LG Bacan was emitted turquoise-to-green colour light after beamed by visible light. The colour was emitted by LG Bacan through the specific polarisation due to coordination bonds of Cu and Ni atoms with O atoms in SiO_2. DG Bacan was less able to emit scattered light when was beamed with visible light due to its low levels of optical activity. That was because the high abundance of other non-Si elements that caused the SiO_2 structure on DG Bacan more symmetrical, by reducing the dipole moment distance of Si–O and increasing the polar covalent bonding length of Si–O. The high abundance of the other elements would lead to the abundance of SiO_2 compounds becomes lower, so the high void space of SiO_2 structure and its capability to rotate planes of incident polarised light into the structure has become less available. All these explanations into evidence amplified that incident light entering the DG Bacan become less visible to be seen, tend to be dark colour, and lack of transparency, due to the less abundance of void space of the structure SiO_2 and less biased.

Crystal Growth Orientation and Size Distribution

The existence of other elements in the Bacan minerals was assumed to inhibit crystal growth orientation in certain directions. It was seen by comparing the orientation of the crystal growth of the DG and LG Bacan (**figure 7c**), which fayalite crystal phase in DG Bacan has an avoided orientation on the [001] direction and LG Bacan have a preferred orientation on the [001] direction. The existence of other elements on the DG Bacan caused the absence of crystal growth orientation in a specific direction and its growth was tended to be evenly distributed to all directions. In mineralogy, orientation of crystal growth direction provides information regarding the mineral formation process. LG Bacan was tend to grow in specific directions which show the process of mineral deposits through the pore - pore with a slow flow rate and flowing in a particular direction only then cooled to form crystals, or commonly referred to groundwater deposits. On DG Bacan, it was possibly formed through pegmatite deposits process in which molten magma containing transition metal elements were mixed with elements of Si and incorporated into the oxide mineral through crystallisation process. This was reinforced by the crystallite size distribution data which presented in **Figure 7**.

Table 5. Average crystallites size and its standard deviation of all crystals phase

Crystal Phase	DG Bacan			LG Bacan			
	SiO_2	$KCaFe_3Si_3O_{12}$	Fe_2SiO_4	SiO_2	$Ca_2CuP_2O_9$	Ni_2SiO_4	$CuSiO_3$
$\bar{L}$ (nm)	64.5986	48.7963	49.2500	21.8054	37.5113	37.8154	37.3204
σ (nm)	15.1494	6.57537	6.35638	0.10188	1.54235	1.77954	1.36374

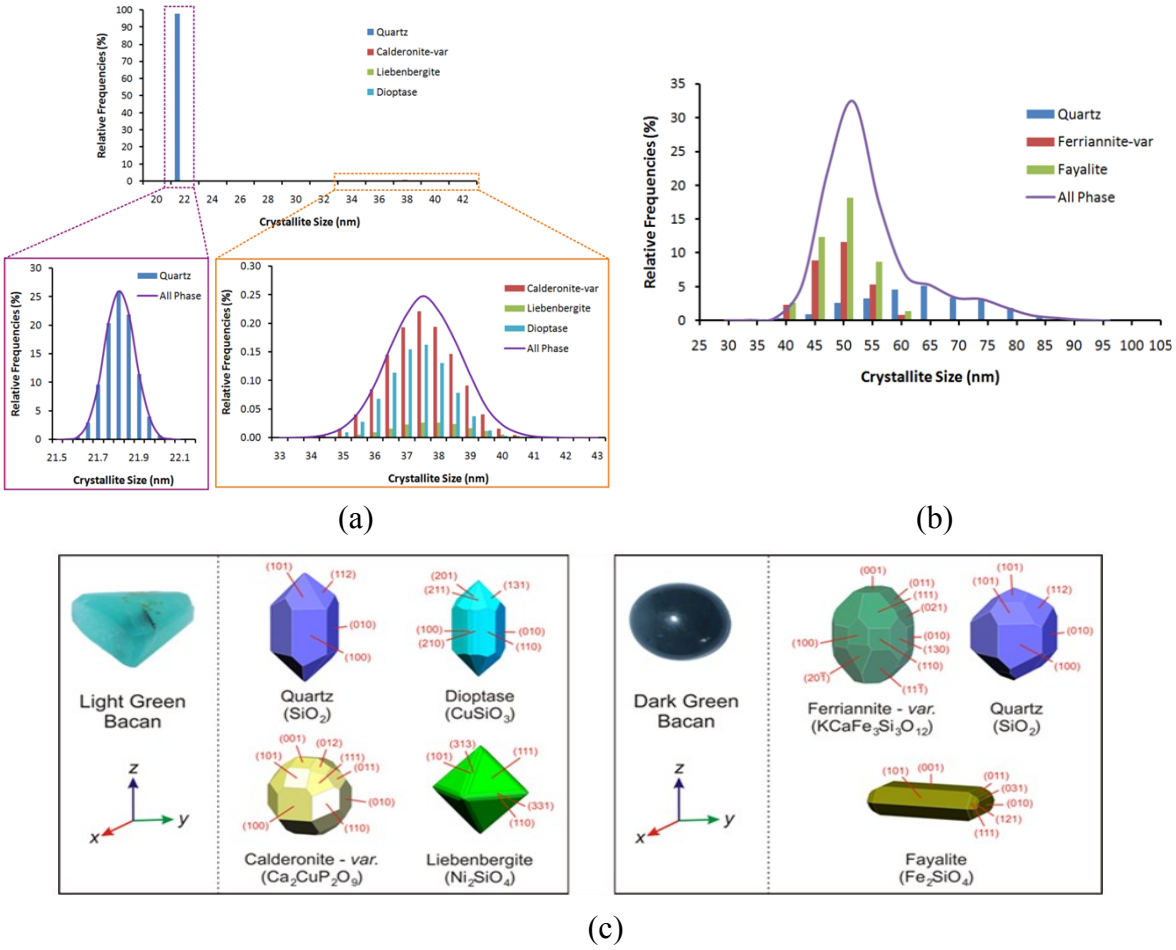

Figure 8. Crystallite size distribution of **(a)** Quartz, Calderonite-var, Dioptase, and Liebenbergite in LG Bacan; and, **(b)** Quartz, Ferriannite-var, and Fayalite in LG Bacan. **(c)** Their crystal shape models.

The crystallite size distribution (**figure 8**; **table 5**) of the LG Bacan was more uniform than DG Bacan, but its size smaller. Data orientation of crystal growth could be attributed with the crystallite size distribution data to draw any conclusions related to the chronology of the material formation. LG Bacan has a small crystallite size, but the size distribution was quite homogenous with orientation of crystal growth in certain directions. LG was possibly formed through groundwater deposits process where the elements forming compounds of Si oxide and other metal oxides, but during the deposit there were incidents or vibrations in the area that caused cracking on the crystal. The position of LG Bacan mineral discovery was not located in deep enough depth of soil, so that it could easily undergo cracking. This caused less transparency of crystal so that the green colour LG Bacan crystal became cloudy. On DG Bacan, its crystallite size was larger, wider crystallite size distribution, and the growth orientation of crystallite was tended to be random, but avoid crystal growth in the direction of [00*l*]. The existence of Fe atoms and other atoms as Si cation substituent on SiO_2 structures inhibit crystal growth in the direction of [001], which the direction as the preferred orientation of SiO_2 crystal growth of LG Bacan. The presence of other elements as Si cation substituent caused SiO_2 formed separated clusters so that growth of crystallite size became larger. Clusters of oxide compounds with the central atoms of Si, Fe, and other atoms causing mineral transparency DG Bacan was not visible and tend to be dark colour. From the physical

looks with the description of crystallite size and orientation of the crystal growth, DG Bacan was possibly formed which caused by quick crystallisation of magma (pegmatite deposits) and formed into a single material.

The difference of representation shape of crystal structure which shown in **Figure 7c** hypothetically caused by both minerals were formed from two different processes. Slower mineral deposits and its growth orientation focused in a particular direction caused the formation of crystal structure be very well-ordered and established specific building of crystal.

CONCLUSION

The depth profiling methods have been done and gives comprehensive representation structure models and the different characters of the two types of Bacan, accurately. LG Bacan is a fascinating mineral which have Dioptase ($CuSiO_3$) and Liebenbergite (Ni_2SiO_4) which contribute releasing turquoise and green colour, respectively; and variant of Calderonite ($Ca_2CuP_2O_9$). DG Bacan is a strong hardness mineral which have Fayalite (Fe_2SiO_4) which contribution to release green-to-dark brown colour and strong hardness level; and variant of Ferriannite ($KCaFe_3Si_3O_{12}$) which contribute to release brownish-to-dark black colour. All crystals phase in LG Bacan has growth orientation on [001] direction, and has more structured crystallite size with small range of its distribution. All phase in DG Bacan has the preferred growth so, except Fayalite crystal phase. DG Bacan less structured than LG Bacan, with wider range of crystallite size distribution, but has harder structure than LG Bacan. Based on geometrical studies, Quartz structure in LG Bacan more polar than DG Bacan, and prospective to be applied piezoelectric materials in electrical application.

ACKNOWLEDGMENT

Authors would like to thank University of Brawijaya for the research funding to Study Centre of Civilisation to undergo research projects of mineral discovery in Indonesia; Drs. Adi Susilo, M.Si., Ph.D. for the constructive suggestions of minerals classification and mineralogical analysis,; Dr. Jazim Hamidi, SH, MH. for the law analysis and prospects of mineral resources discovery in Indonesia to protect in law and raising mineral values for wealth increase of the people in Indonesia; Irham Muhammad, SH, MH. for mineral discovery and sampling; and Ravi Mahesta for technical support. Authors would like to thank to B.A. Hunter and C.J. Howard for Rietica, and W.J. Kaminsky for WinXMorph program providers. No Authors in conflict in all of research process and interest.

REFERENCES

[1] Chattopadhyay, S., Chattopadhyay, D., Chapter 12: Mining Industries and Their Sustainable Management, *in* R. Malhorta, Fossil Energy Selected Entries from the Encyclopedia of Sustainability Science and Technology, **2013**, *Springer*, New York.
[2] Rafferty, J. P., Minerals, **2012**, *Britannica Educational Publishing*, New York.
[3] Borchardt-Ott, W., Crystallography, 3rd Ed., **2011**, *Springer*, Heidelberg.
[4] Ministry of Trade of The Republic of Indonesia, Indonesian Gemstones: Exclusively Captivating, 1st Ed., **2010**, *Trade Research and Development Agency Ministry of Trade*, Republic of Indonesia.
[5] Whitfield, P., Mitchell, L., Chapter 6 : Phase Identification and Quantitative Methods, *in* Clearfield, A., Reibenspies, J.H., Bhuvanesh, N., Principles and Applications of Powder Diffraction, **2008**, *John Wiley & Sons, Ltd.,* Oxford, United Kingdom.
[6] Zolotoyabko, E., *J. Acta Cryst.*, **1986**, 19, 267.

[7] IUCR Powder Diffraction, **1997**, 22, 21.
[8] Howard, C.J., *J. Appl. Cryst.*, **1982**, 15, 615.
[9] Donnay, G., Morimoto, N., Takeda, H., Donnay, J.D.H., *Acta Cryst.*, **1964**, 17, 1369-1373.
[10] del Tanago, J.G., La Iglesia, A., Rius, J., Fernandez Santin, S., *Am. Mineral.*, **2003**, 88, 1703-1708.
[11] della Giusta, A., Ottonello, G., Secco, L., *Acta Cryst. B*, **1990**, 46, 160-165.
[12] le Page, Y., Donnay, G., *Acta Cryst. B*, **1974**, 32, 2456-2459.
[13] Otto, H.H., Meibohm, M., *Z. Kristallogr.*, **1999**, 214, 558-565
[14] Ma, C.B., *Z. Kristallogr. Krist.*, **1975**, 141, 126-137.
[15] Downs, R. T., Hall-Wallace, M., *Am. Mineral.*, **2003**, 88, 247-250.
[16] Kaminsky, W.J., *J. Appl. Cryst.*, **2005**, 38, 566-567.
[17] Kaminsky, W.J., *J. Appl. Cryst.*, **2007**, 40, 382-385.
[18] Larson, A. C., von Dreele, R. B., *Los Alamos Nat. Lab. Report*, LAUR, **2000**, 86, 748.
[19] Balzar, D., Popa, N. C., *The Rigaku J.*, **2005**, 22(1), 16-25.
[20] Lyubomirova, V., Smit, Z., Fajfar, H., Zlateva, B., Djingova, R., Kuleff, I., *Mediterranean Archeol. Archeometry*, **2015**, 15 (2), 257-275.
[21] Supriadi, M.B., Chen, M.C., Li, Y.S., *J. Pure. App. Chem. Res.*, **2013**, 2(1), 1-10.
[22] Nivorozhkin, A.L., Toflund H., *Edu. Chem.*, **1994**, 1, 22-24.
[23] Gautier, R., Klingsporn, J. M., van Duyne, R. P., Poeppelmeier, K. R., *Nature Mater.*, **2016**, 15, 591-592.